Title

In Vitro and In Vivo Characterization of Two C-11-Labeled PET Tracers for Vesicular Acetylcholine Transporter

Journal

Molecular Imaging and Biology, 16(6)

ISSN

1536-1632

Authors

Padakanti, Prashanth K
Zhang, Xiang
Jin, Hongjun
et al.

Publication Date

2014-12-01

DOI

10.1007/s11307-014-0749-9

Peer reviewed

HHS Public Access

Author manuscript

Mol Imaging Biol. Author manuscript; available in PMC 2015 April 21.

Published in final edited form as:

Mol Imaging Biol. 2014 December ; 16(6): 773–780. doi:10.1007/s11307-014-0749-9.

In Vitro and *In Vivo* Characterization of Two C-11-Labeled PET Tracers for Vesicular Acetylcholine Transporter

Prashanth K. Padakanti[1], **Xiang Zhang**[1], **Hongjun Jin**[1], **Jinquan Cui**[1], **Ruike Wang**[1], **Junfeng Li**[1], **Hubert P. Flores**[2], **Stanley M. Parsons**[3], **Joel S. Perlmutter**[1,2], and **Zhude Tu**[1]

[1]Department of Radiology, Washington University School of Medicine, 510 South Kingshighway Blvd., St. Louis, MO, 63110, USA

[2]Department of Neurology, Washington University School of Medicine, 510 South Kingshighway Blvd., St. Louis, MO, 63110, USA

[3]Department of Chemistry and Biochemistry, University of California, Santa Barbara, CA, 93106, USA

Abstract

Purpose—The vesicular acetylcholine transporter (VAChT) is a specific biomarker for imaging presynaptic cholinergic neurons. Herein, two potent and selective ^{11}C-labeled VAChT inhibitors were evaluated in rodents and nonhuman primates for imaging VAChT *in vivo*.

Procedures—For both (−)-[^{11}C]**2** and (−)-[^{11}C]**6**, biodistribution, autoradiography, and metabolism studies were performed in male Sprague Dawley rats. Positron emission tomography (PET) brain studies with (−)-[^{11}C]**2** were performed in adult male cynomolgus macaques; 2 h dynamic data was acquired, and the regions of interest were drawn by co-registration of the PET images with the MRI.

Results—The resolved enantiomers (−)-**2** and (−)-**6** were very potent and selective for VAChT *in vitro* (K_i<5 nM for VAChT with >35-fold selectivity for VAChT *vs*. σ receptors); both radioligands, (−)-[^{11}C]**2** and (−)-[^{11}C]**6**, demonstrated high accumulation in the VAChT-enriched striatum of rats. (−)-[^{11}C]**2** had a higher striatum to cerebellum ratio of 2.4-fold at 60 min; at 30 min, striatal uptake reached 0.550±0.086 %ID/g. Uptake was also specific and selective; following pretreatment with (±)-**2**, striatal uptake of (−)-[^{11}C]**2** in rats at 30 min decreased by 50 %, while pretreatment with a potent sigma ligand had no significant effect on striatal uptake in rats. In addition, (−)-[^{11}C]**2** displayed favorable *in vivo* stability in rat blood and brain. PET studies of (−)-[^{11}C]**2** in nonhuman primates indicate that it readily crosses the blood-brain barrier (BBB) and provides clear visualization of the striatum; striatal uptake reaches the maximum at 60 min, at which time the target to nontarget ratio reached ~2-fold.

Conclusions—The radioligand (−)-[^{11}C]**2** has high potential to be a suitable PET radioligand for imaging VAChT in the brain of living subjects.

Correspondence to: Zhude Tu; tuz@mir.wustl.edu.

Conflict of Interest. The authors declare that they have no conflict of interest.

Keywords

VAChT; Alzheimer's disease; PET imaging; Radiotracer; Vesamicol

Introduction

The vesicular acetylcholine transporter (VAChT), predominantly located in the presynaptic vesicles [1–3], is responsible for the loading of acetylcholine (ACh) into presynaptic vesicles. This has been demonstrated by noncompetitive inhibition of ACh storage when VAChT is bound to *trans*-2-(4-phenylpiperidino)cyclohexanol (vesamicol) [4, 5]; vesamicol binds to VAChT at a site different from the acetylcholine transporter recognition site. Extensive research has revealed that VAChT plays a vital role in the release of ACh and physiological functions in the central nervous system and is highly expressed in the striatum [6]. VAChT is widely accepted as a reliable biomarker for the abnormal cholinergic function, which is associated with the severity of dementia and other neurodegenerative diseases, such as Alzheimer's disease (AD) and Parkinson's disease [7–9].

Positron emission tomography (PET) is a noninvasive imaging modality that can be used to quantify VAChT *in vivo* and study changes in cholinergic function in response to therapy; it is widely applied in the clinical investigation of central nervous system disorders and other diseases [10–14]. In the companion manuscript [15], we reported the synthesis and radiosynthesis of two potent and selective ^{11}C-labeled VAChT inhibitors, (−)-[^{11}C]**2** and (−)-[^{11}C]**6** (Fig. 1). Here, we reported the *in vitro* characterization of the binding affinity of these compounds and the *in vivo* evaluation of the two radioligands in rodents and nonhuman primates (NHPs).

Methods

In Vitro Biological Evaluation

VAChT Binding Affinity Studies—The binding affinity for both enantiomers of each of the two new compounds was determined using *in vitro* competition assays with [^{3}H]vesamicol at a subsaturating concentration of 5 nM for binding to human VAChT present in synaptic-like microvesicles in postnuclear supernatant prepared from PC12$^{A123.7}$ cells [16]. As in our previous studies of VAChT inhibitors, nonspecific binding was determined from samples that contained 1 μM of nonradioactive (±)-vesamicol and test compounds were assayed in increments of 10-fold from 0.1 to 10,000 nM concentration [5, 17–20]. The surfaces of containers were precoated with Sigmacote (Sigma-Aldrich, MO). Samples containing 200 μg postnuclear supernatant in 200 μl of 110 mM potassium tartrate, 20 mM HEPES (pH 7.4 with KOH), 1 mM dithiothreitol, and 0.02 % sodium azide were incubated at 22 °C for 24 h. A volume of 90 μl was filtered in duplicate through GF/F glass fiber filters coated with polyethylenimine and washed. Filter-bound radioactivity was determined by liquid scintillation spectrometry for 10 min per sample. Averaged data were fit by regression analysis with a rectangular hyperbola to estimate K_i. All compounds were independently assayed at least twice.

Sigma Receptor Binding Affinity Study—The σ receptor binding studies were conducted as previously reported [21, 22]. The σ_1 receptor binding assays were performed in 96-well plates using approximately 300 μg protein of guinea pig brain membrane homogenate and 5 nM (+)-[^{3}H]pentazocine (1.30 GBq/μmol, PerkinElmer, Boston, MA); nonspecific binding was determined from samples that contained 10 μM of cold haloperidol. The σ_2 receptor binding assays were similarly performed using rat liver membrane homogenates (~300 μg protein) and ~5 nM [^{3}H]ditolylguanidine (2.15 GBq/μmol, PerkinElmer, Boston, MA) in the presence of 1 μM (+)-pentazocine to block σ_1 sites; nonspecific binding was determined from samples that contained 10 μM of cold haloperidol. Data from these experiments were modeled using nonlinear regression analysis to determine the concentration that inhibits 50 % of the specific binding of the radioligand (IC_{50} value). Competitive binding curves were best fit to a one-site model and gave pseudo-Hill coefficients of 0.6–1.0. K_i values were calculated using the method of Cheng and Prusoff [23] and are presented as the mean±SEM. A K_i value of 7.89 nM for (+)-[^{3}H]pentazocine and guinea pig brain and a K_i value of 30.73 nM for [^{3}H]ditolylguanidine and rat liver were used for these calculations.

Biodistribution, Autoradiography, and Metabolism Studies in Rats

All animal experiments were conducted in compliance with the Guidelines for the Care and Use of Research Animals under protocols approved by Washington University's Animal Studies Committee. For rat biodistribution studies, 10.6 MBq of (−)-[^{11}C]**2** or 5.5 MBq of (−)-[^{11}C]**6** was injected *via* the tail vein into mature male Sprague Dawley (SD) rats (*n*=4 per study group) under 2–3 % isoflurane/oxygen anesthesia. At 2, 30, and 60 min postinjection (p.i.), the rats were again anesthetized and euthanized. In addition to these baseline studies, the specific uptake of (−)-[^{11}C]**2** was evaluated at 30 min p.i. using (±)-**2** to block VAChT and YUN-143 to block $\sigma_{1/2}$ receptors in the brain; blocking agents were injected 2 min before the radiotracer. The whole brain was quickly harvested, the blood was removed by blotting, and regions consisting of the cerebellum, brain stem, thalamus, striatum, cortex, and hippocampus were separated; the remainder of the brain was collected to determine total brain uptake. Peripheral organs and tissues including blood, lung, liver, kidney, muscle, fat and heart, pancreas, and spleen were also collected; all samples were weighed and counted in an automated well counter with a standard dilution of the injectate. Counts were decay-corrected and the %ID/g calculated. The striatum to organ ratios were calculated by dividing the %ID/g of the striatum by the %ID/g of the nontarget brain region. A two-tailed paired Student's *t* test was used to compare striatal uptake (%ID/g) in rats pretreated with the blocking agents *versus* that of control rats. A *p* value of 0.05 was considered statistically significant.

For the *ex vivo* autoradiography study, a mature male SD rat was injected with 115 MBq of (−)-[^{11}C]**2** and euthanized 30 min p.i. as described above. The whole brain was quickly removed and snap-frozen, and 1-mm coronal sections were obtained using a chrome brain matrix (Zivic Instruments Inc., Pittsburg, PA). The brain slices were carefully placed on a clear sheet, covered with film, and counted on an InstantImager (Packard Instrument Company, Meriden, CT). A photographic image was obtained using a flatbed scanner.

Acetylcholine esterase (AChE) staining was performed to confirm striatal distribution of VAChT. The whole brain of a mature male SD rat was snap-frozen, and 20-μm sections obtained using a cryotome were thaw mounted onto glass slides and air-dried. Slides were preincubated in 100 mM sodium acetate buffer, pH 5.2, with 20 mM tetra(monoisopropyl)pyrophosphortetramide (iso-OMPA) for 15 min [24], then transferred into the AChE incubation media (4 mM acetylthiocholine iodide (ASChI), 2 mM copper, 10 mM glycine, and 20 mM iso-OMPA in acetate buffer) for 1 h at 37 °C with constant agitation and rinsed three times with deionized water, each for 1 min. Slides were immediately postincubated for 15 min in 3 % potassium ferricyanide in acetate buffer and again rinsed as described above. Finally, the stained sections were dehydrated and covered with a cover slip for digital photomicrography.

The *in vivo* metabolism of (−)-[^{11}C]**2** was evaluated in rat blood and brain. (−)-[^{11}C]**2**, 30–160 MBq, was injected into male SD rats which were euthanized at 5, 20, 40, and 60 min p.i. HPLC metabolite analysis was performed using solvent extracts of plasma samples and brain homogenates from each rat. For blood metabolite analysis, a 1 ml aliquot of heparinized whole blood was centrifuged to separate plasma from packed red cells; 0.4 ml plasma was extracted and deproteinated with 0.6 ml acetonitrile. This 1.0 ml solvent extract of plasma was centrifuged to precipitate the plasma proteins, and 0.2 ml of the supernatant was diluted with 0.2 ml of distilled water for HPLC analysis. The HPLC was equipped with a 200 μl injection loop and an Agilent SB-C18 analytical column (250×4.6 mm, 5 μm); the mobile phase was 37 % acetonitrile/0.1 M ammonium formate buffer (*v/v*) (pH 4.5), flow rate 1.1 ml/min, and fractions were collected every minute for 16 min. The retention time of the parent compound was ~10 min. HPLC fractions were counted in a well counter, and the counts were decay-corrected. For rat brain metabolite analysis, the whole brain was harvested; excess blood was blotted, the tissue was homogenized on ice, and the radioactivity was extracted by adding 1.2 ml of acetonitrile and homogenizing further. A 1.0 ml aliquot of this brain homogenate was centrifuged to pellet the debris; 0.2 ml of the clear supernatant was diluted with 0.2 ml of distilled water for HPLC injection as described above.

In Vivo MicroPET Imaging of the Male Cynomolgus Monkey Brain

For each study, a 2-h dynamic scan was performed on an adult male cynomolgus macaque (3.5–5 kg); three independent microPET scans were conducted on the same subject to make sure the reproducibility of the data. The scanner used for these studies is a microPET Focus 220 scanner (Concorde/CTI/Siemens Microsystems, Knoxville, TN). A detailed description of the procedures used for similar studies has been previously published [25]. After transportation to the PET scanner suite under ketamine anesthesia, the subject was intubated and a percutaneous venous catheter was placed for radiotracer injection. Anesthesia was maintained at 0.75–2.0 % isoflurane/oxygen throughout the PET scanning procedure. The subject was placed supine on the scanner bed, with the brain in the center of the field of view (FOV). Prior to each microPET scanning session, a brief transmission scan was used to check positioning; after confirmation that the target regions were within the FOV, a 45-min transmission scan was obtained for attenuation correction. Subsequently, 340–480 MBq of

(−)-[^{11}C]**2** was administered *via* the venous catheter; the PET data acquisition protocol is described below.

MicroPET Image Processing and Analysis

PET scans were collected for 120 min beginning with tracer injection and binned to the following time frames: 3 × 1, 4 × 2, 3 × 3, and 20 × 5 min. Emission data were corrected for attenuation, scatter, random data, and dead time. PET image reconstructed resolution was <2.0 mm full width half maximum for all three dimensions at the center of the FOV. Correction for movement of individual frames was unnecessary because the anesthetized animal's head was immobilized. An MR image was co-registered to the PET scan using automatic image registration [26]. 3D regions of interest (ROIs) were manually drawn through all planes of co-registered MR images for the striatum and cerebellum. The ROIs were then overlaid on all reconstructed PET images to obtain time-activity curves. Activity measures were standardized to body weight and dose of radioactivity injected to yield the standardized uptake value (SUV).

Results and Discussion

In Vitro Binding Affinity Studies

In vitro binding affinity studies were performed to measure the affinities of **2** and **6** towards the VAChT and sigma (σ) receptors (Table 1). [^{3}H]Vesamicol was used for the VAChT binding assay; [^{3}H]pentazocine and [^{3}H]DTG in the presence of 1 μM (+)-pentazocine were used for σ_1 and σ_2 receptor binding assays, respectively. Results showed that enantiomer (−)-**2** was more potent than either (+)-**2** or vesamicol, with VAChT K_i values (nM) of 1.6±0.1, 34.0±7.9, and 10.2±1.3 for (−)-**2**, (+)-**2**, and vesamicol, respectively. Similarly, enantiomer (−)-**6** was also more potent with VAChT K_i values (nM) of 3.5±0.3, 38.9±7.4, and 18.6±2.3, respectively, for (−)-**6**, (+)-**6**, and vesamicol, respectively. The selectivity of (−)-**2** for VAChT *versus* σ_1 and σ_2 receptors was >35- and 1,600-fold, respectively, and the selectivity of (−)-**6** for VAChT *versus* σ_1 and σ_2 receptors was >125- and 650-fold, respectively.

Biodistribution Studies in Rats

Biodistribution in peripheral tissues and regional brain distribution studies of (−)-[^{11}C]**2** and (−)-[^{11}C]**6** were performed in adult male SD rats at 2, 30, and 60 min p.i.; the results are shown in Table 2. Rapid initial uptake was observed for both compounds in all organs. For (−)-[^{11}C]**2**, at 2 min p.i., the uptake in total brain was 0.56 %ID/g. Washout by 30 min p.i. was evident and total brain decreased to 0.34 %ID/g; this trend continued at 60 min p.i. Although the initial blood uptake at 2 min was higher than that in the brain, by 30 min p.i., the %ID/g values of 0.25 for blood and 0.34 for brain suggest that the tracer was cleared from the blood but was retained in the brain. For (−)-[^{11}C]**2**, for the peripheral tissues, liver had the highest uptake. The regional brain distribution studies of (−)-[^{11}C]**2** in rats showed the highest and homogeneous uptake at 2 min p.i. with %ID/g values of 0.57 for the cerebellum, brain stem, and thalamus, and 0.56, 0.58, and 0.51 for the striatum, cortex, and hippocampus, respectively (Fig. 2). In subsequent time points, retention was the highest in the striatum for (−)-[^{11}C]**2** with 0.55 and 0.36 %ID/g at 30 and 60 min. In other brain

regions, retention was low to moderate with %ID/g values of 0.28, 0.37, 0.32, 0.31, and 0.31 at 30 min p.i. and 0.15, 0.23, 0.19, 0.19, and 0.19 at 60 min p.i. in the cerebellum, brain stem, thalamus, cortex, and hippocampus, respectively. These results are consistent with the reported distribution of VAChT in the rat brain, in which striatal tissue is VAChT enriched. Washout was rapid in the cerebellum, the accepted nontarget brain region for VAChT. The uptake ratios in the striatum *versus* the cerebellum increased significantly over time, from unity at 2 min to 2.4-fold at 60 min p.i. The pyridine tracer (−)-[^{11}C]**6** also showed the highest accumulation in the striatum compared to the other brain regions of interest (Fig. 2), including the cerebellum, brain stem, thalamus, cortex, and hippocampus at 5, 30, and 60 min; however, the uptake (%ID/g) ratios of the striatum to cerebellum was only 1.6 at 60 min p.i. Among the peripheral tissues, the highest uptake of (−)-[^{11}C]**6** was also observed in the liver.

The *in vivo* specific binding of (−)-[^{11}C]**2** and (−)-[^{11}C]**6** in rat brain was evaluated through blocking studies in male SD rats which were pretreated with either the potent and nonselective $\sigma_{1/2}$ ligand *N*-(4′-fluorobenzyl)-4-(3-bromophenyl)acetamide (YUN-143) ($K_{i-\sigma1}$=1.2±0.2 nM; $K_{i-\sigma2}$=6.1±1.5 nM) [27] or the VAChT ligand (±)-**2** $K_{i-VAChT}$=4.64±0.47 nM, $K_{i-\sigma1}$= 32±10 nM, and $K_{i-\sigma2}$ > 1,500 nM. Blocking agents were administered by i.v. 1 min prior to tracer injection, and uptake was evaluated 30 min p.i. Pretreatment with the YUN-143 (2 mg/kg) did not result in any significant decrease in striatal accumulation of radioactivity in the rats compared to control rats (p>0.05). In contrast, pretreatment with VAChT ligand (±)-**2** (1 mg/kg) resulted in significant decrease in uptake; the striatal accumulation of the radioactivity in the pretreated rats was reduced by 50 % compared to those without pretreatment (Table 3, p=0.0014). Pretreatment of rats with (±)-**2** prior to injection of (−)-[^{11}C]**6** suggested lower specific binding to VAChT; the striatal accumulation showed 20 % reduction compared to the control rats (p=0.025), which was much less than the reduction seen for (−)-[^{11}C]**2**.

Ex Vivo Autoradiography Study in the Rat Brain

In order to demonstrate selective accumulation of (−)-[^{11}C]**2** in rat striatal regions, *ex vivo* autoradiography study was performed. At 30 min p.i. of (−)-[^{11}C]**2** injection (115 MBq), a rat was euthanized, and the brain was quickly removed, snap-frozen, and sliced into 1-mm coronal sections. The brain sections were counted on a Packard InstantImager for 5 h. Regions of interest were manually drawn. The data suggested the highest accumulation of (−)-[^{11}C]**2** was in the VAChT-enriched striatum. The ratio of radioactivity in the striatum/cortex reached 1.7, which is consistent with the biodistribution data (1.79±0.32, 30 min p.i.). Acetylcholine esterase (AChE) staining on a control rat following a reported procedure [28] confirmed that striatal AChE activity is significantly higher than that in the cortex (Fig. 3).

Metabolism Study in Rats

The metabolism study of (−)-[^{11}C]**2** in rat blood and brain was performed inmale SD rats at 5, 20, 40, and 60 min p.i. Both the blood and brain samples were processed, and solvent extracts were injected on a reverse-phase HPLC system. HPLC fractions were collected and the radioactivity was counted on a well counter. Three radioactive peaks were observed in the blood samples with retention times of 3, 6, and 10 min, which correspond to metabolite

1, metabolite 2, and the parent compound (−)-[^{11}C]**2**, respectively. At 60 min p.i., 62 % of the radioactivity in plasma was the parent compound; metabolites 1 and 2 were 19 % each. Metabolite analysis of brain samples showed that 77 % of the radioactivity was the parent compound at 60 min p.i. The stable metabolic profile suggested that (−)-[^{11}C]**2** is suitable for further evaluation as a PET tracer for imaging VAChT *in vivo*.

MicroPET Imaging Studies in the NHP Brain

Preliminary studies of (−)-[^{11}C]**2** in rodents have shown that this new PET radiotracer can be potentially used to measure VAChT density *in vivo*. Therefore, microPET brain imaging studies of (−)-[^{11}C]**2** were performed in male cynomolgus macaques (n = 3) to assess its potential as an imaging agent to measure VAChT density (Fig. 4). The microPET studies demonstrated that (−)-[^{11}C]**2** readily enters the brain and accumulates in the striatum. Averaged tissue time-activity curves revealed that the results of these studies can be reproduced and that the tracer showed suitable wash-in and wash-out kinetics, in that the radioactivity accumulation reached maximum at around 60 min of tracer injection. The ratio of radioactivity accumulation in the target (striatum) and nontarget (cerebellum) increases gradually and reaches ~2-fold at 60 min p.i. This data is in reasonable agreement with the rat studies, which further suggests that this new compound is a promising PET tracer to image VAChT *in vivo*.

In 2010, Giboureau *et al*. published a comprehensive review of PET radioligands for imaging VAChT [9]. Although numerous compounds have been developed as potential PET ligands for imaging VAChT, less than ten have been evaluated in NHP or human subjects [25, 29–40]. Very few are still considered potential candidates for clinical studies due to problems including poor selectivity over σ receptors, rapid metabolism, defluorination, low extraction from the blood, and slow brain kinetics that require a long time to reach pseudoequilibrium [7, 9]. Vesamicol and many analogues which are even more potent inhibitors of VAChT also bind to σ receptors [41–43] and nonvesicular vesamicol binding protein, and thus lack selectivity [44]. Although (−)-*o*-[^{11}C]methylvesamicol ((−)-[^{11}C]OMV) had high binding affinity for VAChT in the brain of conscious NHP, it also bound to σ_1 receptors [45]. In contrast, the regional brain distribution of (−)-[^{18}F]FEOBV was unaffected by pretreatment with haloperidol or (1)-3-PPP in rodents, suggesting it does not bind to dopamine or σ_1 receptors [46]. However, although it has been approved for human studies, (−)-[^{18}F]FEOBV displays very slow striatal equilibrium kinetics in both NHP and human: after 90 min, pseudoequilibrium was not reached in the striatum; striatal accumulation continued to increase for 180 min p.i. in NHP [36] and for 240 min p.i. in normal human subjects [38]. Based on our initial *in vitro* characterization and the preliminary *in vivo* evaluation in rodent and NHP reported in this manuscript, we conclude (−)-[^{11}C]**2** is a promising candidate for imaging VAChT.

Conclusion

The biodistribution and regional brain uptake of (−)-[^{11}C]**2** and (−)-[^{11}C]**6** were evaluated in rats as PET ligands for imaging VAChT and microPET brain imaging studies with (−)-[^{11}C]**2** were subsequently conducted in nonhuman primates. Biodistribution evaluation in rat

studies revealed that both radiotracers penetrated the blood-brain barrier (BBB). (−)-[^{11}C]**2** revealed good brain penetration, high target to nontarget ratios, and suitable washout kinetics in both rodents and NHPs. Although (−)-**6** displayed potent binding towards VAChT and high selectivity over σ_1 receptor in *in vitro* studies, it did not show selective binding in the rat brain, perhaps related to the somewhat lower affinity for VAChT than that of (−)-[^{11}C]**2**. Based on our data, we conclude that (−)-[^{11}C]**2** is a potential PET tracer for quantifying VAChT *in vivo*. Future studies will determine if this tracer can be used in clinical studies for imaging VAChT.

Acknowledgments

This work was supported by NIH grants NS061025, NS075527, and MH092797. The authors thank John Hood, Christina Zukas, and Darryl Craig for their assistance with the nonhuman primate microPET studies.

Abbreviation

ACh	Acetylcholine
AChE	Acetylcholine esterase
ASChI	Acetylthiocholine iodide
Anal	Analysis
BBB	Blood-brain barrier
DTG	1,3-Di-*o*-tolylguanidine
%ID/g	Percent injected dose per gram
iso-OMPA	Tetra(monoisopropyl)pyrophosphortetramide
MRI	Magnetic resonance imaging
PET	Positron emission tomography
p.i.	Post injection
ROIs	Regions of interest
SD	Sprague Dawley
VAChT	Vesicular acetylcholine transporter
Vesamicol	*trans*-2-(4-Phenylpiperidino)cyclohexanol

References

1. Gilmor ML, Nash NR, Roghani A, et al. Expression of the putative vesicular acetylcholine transporter in rat brain and localization in cholinergic synaptic vesicles. J Neurosci: Off J Soc Neurosci. 1996; 16:2179–2190.
2. Erickson JD, Varoqui H, Schafer MK, et al. Functional identification of a vesicular acetylcholine transporter and its expression from a “cholinergic” gene locus. J Biol Chem. 1994; 269:21929–21932. [PubMed: 8071310]
3. Roghani A, Feldman J, Kohan SA, et al. Molecular cloning of a putative vesicular transporter for acetylcholine. Proc Natl Acad Sci USA. 1994; 91:10620–10624. [PubMed: 7938002]

4. Bahr BA, Parsons SM. Acetylcholine transport and drug inhibition kinetics in Torpedo synaptic vesicles. J Neurochem. 1986; 46:1214–1218. [PubMed: 3950625]
5. Rogers GA, Parsons SM, Anderson DC, et al. Synthesis, in vitro acetylcholine-storage-blocking activities, and biological properties of derivatives and analogues of trans-2-(4-phenylpiperidino)cyclohexanol (vesamicol). J Med Chem. 1989; 32:1217–1230. [PubMed: 2724295]
6. Prado VF, Martins-Silva C, de Castro BM, et al. Mice deficient for the vesicular acetylcholine transporter are myasthenic and have deficits in object and social recognition. Neuron. 2006; 51:601–612. [PubMed: 16950158]
7. Efange SM. In vivo imaging of the vesicular acetylcholine transporter and the vesicular monoamine transporter. FASEB J: Off Publ Fed Am Soc Exp Biol. 2000; 14:2401–2413.
8. Gilmor ML, Erickson JD, Varoqui H, et al. Preservation of nucleus basalis neurons containing choline acetyltransferase and the vesicular acetylcholine transporter in the elderly with mild cognitive impairment and early Alzheimer's disease. J Comp Neurol. 1999; 411:693–704. [PubMed: 10421878]
9. Giboureau N, Som IM, Boucher-Arnold A, Guilloteau D, Kassiou M. PET radioligands for the vesicular acetylcholine transporter (VAChT). Curr Top Med Chem. 2010; 10:1569–1583. [PubMed: 20583990]
10. Garnett ES, Firnau G, Nahmias C. Dopamine visualized in the basal ganglia of living man. Nature. 1983; 305:137–138. [PubMed: 6604227]
11. Antonini A, Leenders KL, Eidelberg D. [^{11}C]raclopride-PET studies of the Huntington's disease rate of progression: relevance of the trinucleotide repeat length. Ann Neurol. 1998; 43:253–255. [PubMed: 9485067]
12. Banati RB, Newcombe J, Gunn RN, et al. The peripheral benzodiazepine binding site in the brain in multiple sclerosis: quantitative in vivo imaging of microglia as a measure of disease activity. Brain:J Neurol. 2000; 123:2321–2337.
13. Choi SR, Golding G, Zhuang Z, et al. Preclinical properties of ^{18}F-AV-45: a PET agent for Abeta plaques in the brain. J Nucl Med: Of Publ Soc Nucl Med. 2009; 50:1887–1894.
14. Rowe CC, Ackerman U, Browne W, et al. Imaging of amyloid beta in Alzheimer's disease with ^{18}F-BAY94-9172, a novel PET tracer: proof of mechanism. Lancet Neurol. 2008; 7:129–135. [PubMed: 18191617]
15. Padakanti PK, Zhang X, Li J, Parsons SM, Perlmutter JS, Tu Z. Syntheses and radiosyntheses of two carbon-11 labeled potent and selective radioligands for imaging vesicular acetylcholine transporter. Mol Imaging Biol. 2014
16. Zea-Ponce Y, Mavel S, Assaad T, et al. Synthesis and in vitro evaluation of new benzovesamicol analogues as potential imaging probes for the vesicular acetylcholine transporter. Bioorg Med Chem. 2005; 13:745–753. [PubMed: 15653342]
17. Efange SM, Khare AB, von Hohenberg K, Mach RH, Parsons SM, Tu Z. Synthesis and in vitro biological evaluation of carbonyl group-containing inhibitors of vesicular acetylcholine transporter. J Med Chem. 2010; 53:2825–2835. [PubMed: 20218624]
18. Wang W, Cui J, Lu X, et al. Synthesis and in vitro biological evaluation of carbonyl group-containing analogues for sigma-1 receptors. J Med Chem. 2011; 54:5362–5372. [PubMed: 21732626]
19. Tu ZD, Wang W, Cui JQ, et al. Synthesis and evaluation of in vitro bioactivity for vesicular acetylcholine transporter inhibitors containing two carbonyl groups. Bioorg Med Chem. 2012; 20:4422–4429. [PubMed: 22739089]
20. Li J, Zhang X, Zhang Z, et al. Heteroaromatic and aniline derivatives of piperidines as potent ligands for vesicular acetylcholine transporter. J Med Chem. 2013; 56:6216–6233. [PubMed: 23802889]
21. Tu Z, Xu J, Jones LA, et al. Fluorine-18-labeled benzamide analogues for imaging the sigma 2 receptor status of solid tumors with positron emission tomography. J Med Chem. 2007; 50:3194–3204. [PubMed: 17579383]

22. Xu J, Tu Z, Jones LA, Vangveravong S, Wheeler KT, Mach RH. [^{3}H]N-[4-(3,4-Dihydro-6,7-dimethoxyisoquinolin-2(1H)-yl)butyl]-2-methoxy-5-methylbenzamide: a novel sigma-2 receptor probe. Eur J Pharmacol. 2005; 525:8–17. [PubMed: 16289030]
23. Cheng Y, Prusoff WH. Relationship between the inhibition constant (K_1) and the concentration of inhibitor which causes 50%inhibition (I_{50}) of an enzymatic reaction. Biochem Pharmacol. 1973; 22:3099–3108. [PubMed: 4202581]
24. Aldridge WN. The differentiation of true and pseudo cholinesterase by organophosphorus compounds. Biochem J. 1953; 53:62–67. [PubMed: 13032034]
25. Tu Z, Efange SM, Xu J, et al. Synthesis and in vitro and in vivo evaluation of ^{18}F-labeled positron emission tomography (PET) ligands for imaging the vesicular acetylcholine transporter. J Med Chem. 2009; 52:1358–1369. [PubMed: 19203271]
26. Woods RP, Mazziotta JC, Cherry SR. MRI-PET registration with automated algorithm. J Comput Assist Tomogr. 1993; 17:536–546. [PubMed: 8331222]
27. Mach RH, Huang Y, Buchheimer N, et al. [^{18}F]N-(4'-Fluorobenzyl)-4-(3-bromophenyl) acetamide for imaging the sigma receptor status of tumors: comparison with [^{18}F]FDG, and [^{125}I]IUDR. Nucl Med Biol. 2001; 28:451–458. [PubMed: 11395319]
28. NAIK NT. Technical variations in Koelle's histochemical method for demonstrating cholinesterase activity. Quart. J Microsc Sci. 1963
29. Shiba K, Nishiyama S, Tsukada H, et al. The potential of (−)-o-[^{11}C]methylvesamicol for diagnosing cholinergic deficit dementia. Synapse. 2009; 63:167–171. [PubMed: 19021207]
30. Widen L, Eriksson L, Ingvar M, Parsons SM, Rogers GA, Stone-Elander S. Positron emission tomographic studies of central cholinergic nerve terminals. Neurosci Lett. 1992; 136:1–4. [PubMed: 1321961]
31. Mach RH, Voytko ML, Ehrenkaufer RL, et al. Imaging of cholinergic terminals using the radiotracer [^{18}F](+)-4-fluorobenzyltrozamicol: in vitro binding studies and positron emission tomography studies in nonhuman primates. Synapse. 1997; 25:368–380. [PubMed: 9097396]
32. Voytko ML, Mach RH, Gage HD, Ehrenkaufer RL, Efange SM, Tobin JR. Cholinergic activity of aged rhesus monkeys revealed by positron emission tomography. Synapse. 2001; 39:95–100. [PubMed: 11071714]
33. Gage HD, Gage JC, Tobin JR, et al. Morphine-induced spinal cholinergic activation: in vivo imaging with positron emission tomography. Pain. 2001; 91:139–145. [PubMed: 11240086]
34. Gage HD, Voytko ML, Ehrenkaufer RL, Tobin JR, Efange SM, Mach RH. Reproducibility of repeated measures of cholinergic terminal density using. J Nucl Med: Off Publ Soc Nucl Med. 2000; 41:2069–2076.
35. Efange SM, Nader MA, Ehrenkaufer RL, et al. (+)-p-([^{18}F]Fluorobenzyl)spirotrozamicol [(+)-[^{18}F]spiro-FBT]: synthesis and biological evaluation of a high-affinity ligand for the vesicular acetylcholine transporter (VAChT. Nucl Med Biol. 1999; 26:189–192. [PubMed: 10100218]
36. Kilbourn MR, Hockley B, Lee L, et al. Positron emission tomography imaging of (*2R*,*3R*)-5-[^{18}F]fluoroethoxybenzovesamicol in rat and monkey brain: a radioligand for the vesicular acetylcholine transporter. Nucl Med Biol. 2009; 36:489–493. [PubMed: 19520289]
37. Giboureau N, Emond P, Fulton RR, et al. Ex vivo and in vivo evaluation of (2*R*,3*R*)-5-[^{18}F]-fluoroethoxy- and fluoropropoxy-benzovesamicol, as PET radioligands for the vesicular acetylcholine transporter. Synapse. 2007; 61:962–970. [PubMed: 17787004]
38. Petrou M, Frey KA, Kilbourn MR, et al. In vivo imaging of human cholinergic nerve terminals with (−)-5-^{18}F-fluoroethoxybenzovesamicol: biodistribution, dosimetry, and tracer kinetic analyses. J Nucl Med: Off Publ Soc Nucl Med. 2014; 55:396–404.
39. Nishiyama S, Ohba H, Kobashi T. Development of novel PET probe [^{11}C](*R*,*R*)HAPT and its stereoisomer [^{11}C](*S*,*S*)HAPT for vesicular acetylcholine transporter imaging: a PET study in conscious monkey. Synapse. 2014
40. Ingvar M, Stone-Elander S, Rogers GA, et al. Striatal D2/acetylcholine interactions: PET studies of the vesamicol receptor. Neuroreport. 1993; 4:1311–1314. [PubMed: 8260611]
41. Custers FG, Leysen JE, Stoof JC, Herscheid JD. Vesamicol and some of its derivatives: questionable ligands for selectively labelling acetylcholine transporters in rat brain. Eur J Pharmacol. 1997; 338:177–183. [PubMed: 9456000]

42. Efange SM, Mach RH, Smith CR, et al. Vesamicol analogues as sigma ligands. Molecular determinants of selectivity at the vesamicol receptor. Biochem Pharmacol. 1995; 49:791–797. [PubMed: 7702637]

43. Shiba K, Ogawa K, Ishiwata K, Yajima K, Mori H. Synthesis and binding affinities of methylvesamicol analogs for the acetylcholine transporter and sigma receptor. Bioorg Med Chem. 2006; 14:2620–2626. [PubMed: 16434200]

44. Hicks BW, Rogers GA, Parsons SM. Purification and characterization of a nonvesicular vesamicol-binding protein from electric organ and demonstration of a related protein in mammalian brain. J Neurochem. 1991; 57:509–519. [PubMed: 1649250]

45. Kawamura K, Shiba K, Tsukada H, Nishiyama S, Mori H, Ishiwata K. Synthesis and evaluation of vesamicol analog (−)-*O*-[^{11}C]methylvesamicol as a PET ligand for vesicular acetylcholine transporter. Ann Nucl Med. 2006; 20:417–424. [PubMed: 16922470]

46. Mulholland GK, Wieland DM, Kilbourn MR, et al. [^{18}F]Fluoroethoxy-benzovesamicol, a PET radiotracer for the vesicular acetylcholine transporter and cholinergic synapses. Synapse. 1998; 30:263–274. [PubMed: 9776130]

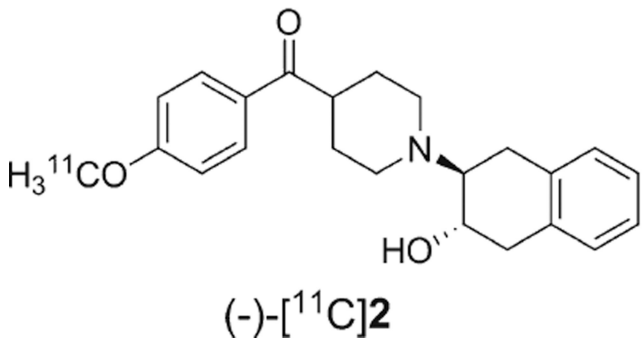

(-)-[^{11}C]**2**

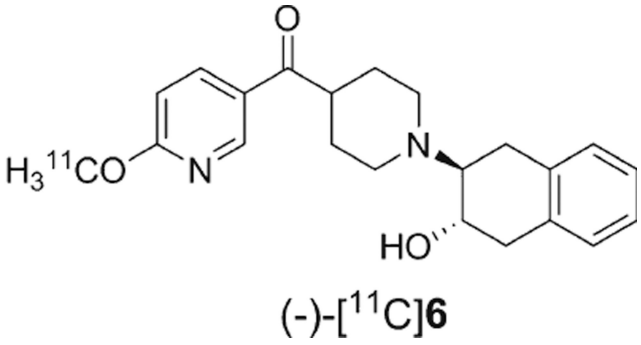

(-)-[^{11}C]**6**

Fig. 1.
Structures of VAChT PET tracers.

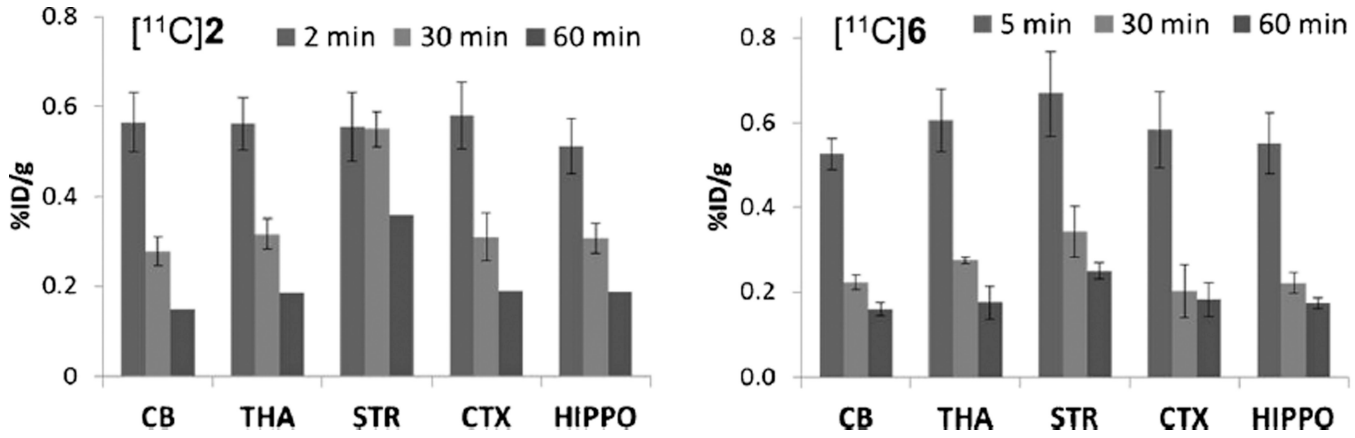

Fig. 2.

Regional brain uptake of (−)-[^{11}C]**2** and (−)-[^{11}C]**6** in SD rat. (−)-[^{11}C]**2** displayed high accumulation in the striatum (*STR*) and fast washout in nontarget regions such as the cerebellum (*CB*), thalamus (*THA*), cortex (*CTX*), and hippocampus (*HIPPO*); the uptake ratio in STR *versus* CB reached 2.4-fold at 60 min p.i. (−)-[^{11}C]**6** also showed the highest uptake in the striatum; however, the ratio was only 1.6-fold at 60 min p.i.

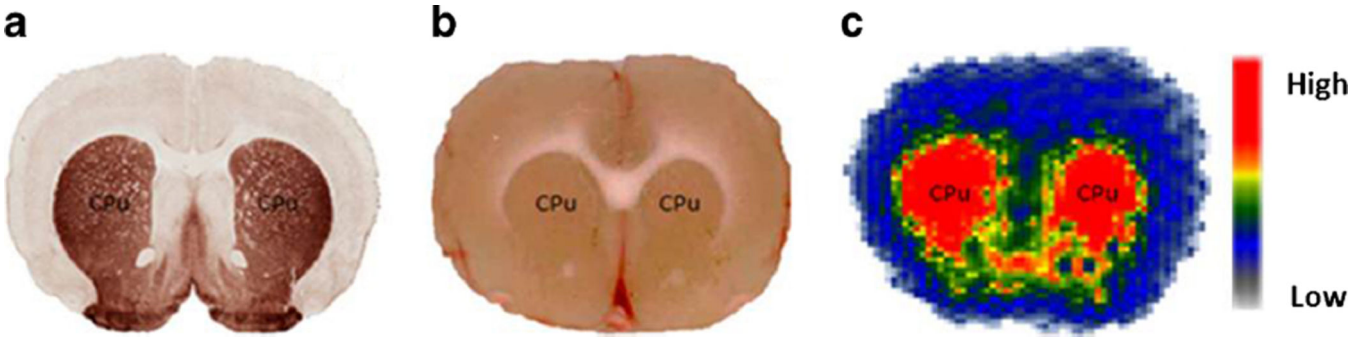

Fig. 3.

Autoradiography study of (−)-[^{11}C]**2** in male SD rat: 115 MBq of (−)-[^{11}C]**2** was administrated into the rat by tail i.v. injection. The animals were euthanized at 30 min under anesthesia p.i. **a** AChE staining, **b** scanned brain slice before autoradiography counting, **c** InstantImager autoradiography. The caudate and putamen regions were noted with *CPu* in all images.

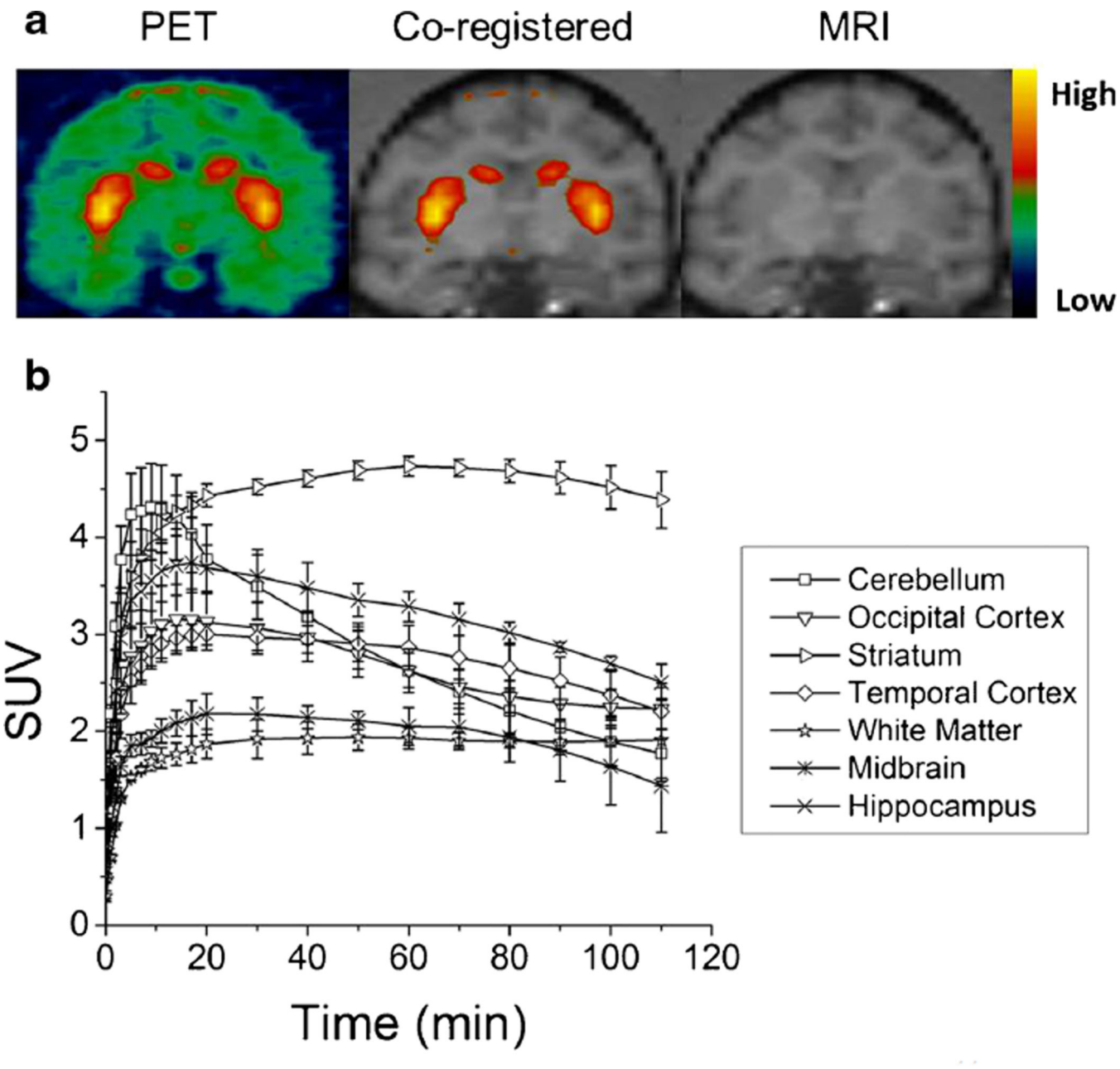

Fig. 4.

A representative microPET image (**a**) and an averaged time-activity curve (**b**) of (−)-[^{11}C]**2** in cynomolgus monkey brain. **a**. microPET images (*left*), co-registered images (*middle*), and MR images (*right*). High uptake of (−)-[^{11}C]**2** in the striatum produced clear visualization of the tracer in the putamen and caudate. **b**. The averaged time-activity curve from three microPET scans demonstrated a good reproducibility for (−)-[^{11}C]**2**.

Table 1

Binding affinities of the final compounds (K_i±SD)

Compound	$K_{i-VAChT}$ (nM)	$K_{i-\sigma1}$ (nM)	$K_{i-\sigma2}$ (nM)	$K_{i-\sigma1}/K_{i-VAChT}$	$K_{i-\sigma2}/K_{i-VAChT}$
(−)-**2**	1.6±1.0	62.1±2.6	2,586±197	38.8	1616
(+)-**2**	34.0±8.0	131±6.5	1,487±63	3.85	43.7
(−)-**6**	3.5±0.3	446±61	2319±236	127	663
(+)-**6**	38.9±7.5	396±36	768±29	10.1	19.7

Table 2

Biodistribution of (−)-[^{11}C]**2** and (−)-[^{11}C]**6** in male Sprague Dawley rats

Organ	2 min	30 min	60 min	5 min	30 min	60 min
	(−)-[^{11}C]2			(−)-[^{11}C]6		
Blood	0.760±0.070	0.248±0.053	0.206±0.025	0.305±0.028	0.162±0.009	0.177±0.008
Lung	1.963±0.147	0.578±0.051	0.340±0.059	1.111±0.119	0.701±0.065	0.559±0.017
Liver	3.632±0.189	2.561±0.243	1.704±0.230	2.689±0.158	1.455±0.091	1.553±0.051
Spleen	1.293±0.047	0.523±0.051	0.350±0.058	1.024±0.106	0.551±0.026	0.470±0.021
Kidney	1.241±0.135	0.651±0.071	0.472±0.040	1.080±0.089	0.854±0.051	0.757±0.071
Pancreas	1.183±0.113	1.116±0.126	0.714±0.159	1.107±0.058	0.694±0.192	0.664±0.086
Muscle	0.202±0.028	0.136±0.007	0.094±0.011	0.180±0.011	0.204±0.013	0.161±0.009
Fat	0.201±0.059	0.710±0.130	0.618±0.147	0.169±0.031	0.375±0.031	0.280±0.067
Heart	0.616±0.062	0.224±0.028	0.156±0.018	0.421±0.023	0.250±0.034	0.202±0.003
Total brain	0.560±0.073	0.337±0.032	0.201±0.036	0.574±0.067	0.247±0.036	0.178±0.015

%ID/g values (mean ± SD) with four rats per group

Mol Imaging Biol. Author manuscript; available in PMC 2015 April 21.

Table 3

The distribution of (−)-[^{11}C]**2** and (−)-[^{11}C]**6** in Sprague Dawley control rats and rats pretreated using a σ ligand, YUN-143, or cold (±)-**2** at 30 min postinjection

Organ	(−)-[^{11}C]2			(−)-[^{11}C]6	
	Control	σ block	VAChT block	Control	VAChT block
Blood	0.309±0.017	0.339±0.075	0.271±0.093	0.162±0.009	0.170±0.014
Lung	1.045±0.091	0.928±0.199	0.927±0.319	0.701±0.065	0.782±0.055
Liver	2.448±0.272	1.962±0.306	2.234±0.258	1.455±0.091	1.048±0.698
Spleen	0.662±0.083	0.515±0.095	0.587±0.154	0.551±0.026	0.599±0.056
Kidney	0.785±0.119	0.751±0.093	0.770±0.113	0.854±0.051	0.892±0.057
Pancreas	1.200±0.105	0.799±0.133	0.764±0.075	0.694±0.192	0.577±0.018
Muscle	0.208±0.010	0.208±0.025	0.242±0.037	0.204±0.013	0.205±0.004
Fat	1.768±0.436	2.020±0.598	1.539±0.761	0.375±0.031	0.314±0.092
Heart	0.290±0.016	0.298±0.048	0.245±0.041	0.250±0.034	0.250±0.019
Cerebellum	0.317±0.047	0.216±0.020	0.214±0.062	0.223±0.016	0.207±0.020
Brain stem	0.437±0.039	0.293±0.037	0.276±0.048	0.257±0.019	0.236±0.020
Thalamus	0.370±0.043	0.280±0.036	0.234±0.038	0.275±0.008	0.235±0.025
Striatum	0.546±0.071	0.629±0.060*	0.276±0.065**	0.342±0.060	0.251±0.013***
Cortex	0.331±0.128	0.292±0.047	0.239±0.100	0.202±0.062	0.218±0.030
Hippocampus	0.350±0.042	0.288±0.020	0.220±0.058	0.222±0.025	0.237±0.014
Total brain	0.370±0.031	0.308±0.021	0.242±0.062	0.247±0.036	0.233±0.014

%ID/g values (mean ± SD) with n = 4 rats per group. p value was determined by using two-tailed paired Student's t test for the striatum uptake in control rats *versus* rats pretreated with the blocking agent

* p>0.05;

** p=0.0014;

*** p=0.025